P. Bajpai
Research Assistant
The University of Toledo,
Toledo, OH 43607

A. Kahraman
Mem. ASME
Associate Professor,
The Ohio State University,
Columbus, OH 43210
e-mail: kahraman.1@osu.edu

N. E. Anderson
Fellow ASME
Staff Engineer,
General Motors Powertrain,
Wixom, MI 48393

A Surface Wear Prediction Methodology for Parallel-Axis Gear Pairs

In this study, a surface wear prediction methodology for spur and helical gears is proposed. The methodology employs a finite elements-based gear contact mechanics model in conjunction with the Archard's wear formulation to predict wear of contacting tooth surfaces. An iterative numerical procedure is developed to account for the changes in the gear contact as the gears wear. A methodology is developed to import gear coordinate measurement machine data into the gear contact model in order to analyze gears with actual manufactured surfaces with profile and lead modifications. Results of an experimental study are presented for validation of the methodology. A set of simulations is also included to highlight the differences between gear pairs having modified and unmodified tooth surfaces, with and without manufacturing errors in terms of their wear characteristics. [DOI: 10.1115/1.1691433]

1 Introduction

Surface wear is considered to be one of the four major failure modes in gear systems, the other three being tooth bending fatigue, contact fatigue, and scoring. The impact of wear on operational life of any gear system has far reaching consequences as gears are essential components of almost every power transmission system. Apart from the direct material loss, that leads to functional failure, surface wear also causes the gear system to change its vibration and noise characteristics significantly [1–3]. Surface wear can also affect the patterns of gear contact in such a way that it can alter stresses and load distribution to accelerate the occurrence of other failure modes [4]. Hence, a better understanding of mechanisms of gear wear including its impact on noise and durability is essential. In addition, the knowledge of the sensitivity of design parameters and manufacturing errors on wear becomes crucial for a gear designer who attempts to minimize wear.

A large number of parameters of the system must be taken into account to describe wear characteristics of contacting surfaces reasonably well. Mechanisms of gear wear are even more complex as the mechanics of gear contact are dictated not only by the geometry, but also by both contact and tooth deformations. In addition, most automotive and aerospace gearing applications operate in mixed or boundary elastohydrodynamic (EHD) lubrication regimes where asperity contacts are possible [5]. Hence, parameters influencing the lubricant film properties are also critical. In addition, the changes in gear tooth geometry as a result of wear results in changes the meshing contact conditions, and, hence, gear contact and tooth bending stresses. Therefore, using stress values corresponding to unworn profiles can result in unrealistic life predictions, requiring knowledge of the progression of wear.

Surface wear has attracted the attention of many researchers over the last fifty years. Attempts were made to predict wear using a simple design equation, but due to the large number of variables that affect the wear phenomenon, a single, widely accepted wear model has not been established. Sliding wear of a dry or lubricated surface can be described by the initial value problem [6–10]

$$\frac{dh}{ds} = F(P, u, \ldots) \tag{1}$$

where h is the wear depth, s is the relative sliding distance, and F

is a function of a number of parameters influencing wear including contact pressure P, sliding velocity u, and hardness, surface roughness, and lubricant related parameters. Wear accumulation can be calculated by integrating Eq. (1), provided that the function F is known. Archard [10] proposed a simple model that that takes probability of asperity collision into account in the form of a wear coefficient k. Although many researchers [11–14] proposed, over the years, more advanced wear models using different methodologies and parameters sets, Archard's wear model still remains the most commonly used model for practical applications, primarily because it is easy to apply. Application examples of Archard's wear model include cam wear [15] and engine piston ring wear [16].

Studies on gear wear are rather sparse. Papers by Flodin and Andersson [7–8] appear to be the first detailed theoretical gear wear studies. In their spur gear wear model [7], they calculated the sliding distance from involute profile geometry. They determined the load carried by each tooth pair in the mesh and calculated contact pressures using a simplified Winkler's mattress model where a surface represented by independent springs carrying the load. Flodin and Anderson [8] stated that this model is not as limited as Hertz' model as nonsmooth surface can be handled, while it is more demanding computationally. The values of contact pressure and sliding distance were then combined in Archard's wear model to determine the wear profile in involute direction. The contact pressure calculations were repeated incrementally to account for the changes in pressure due to wear of the contacting surfaces. Flodin and Andersson later extended their spur gear wear methodology to helical gears [8,17] by slicing the helical gear in the face direction into narrow spur gear segments staggered according to the helix angle. These studies form a solid basis for prediction of gear wear. However, several potentially significant factors are yet to be investigated. For instance, the influence of intentional tooth surface modifications has not been included in these studies, while almost all real gears have some kind of intended modification scheme that deviates the surface from a perfect involute surface typically through material removal. Tooth modifications influence the contact pattern, load distribution, and contact stresses significantly as reported previously [18]. Similarly, while the nominal geometry of mating surfaces is very important for any wear prediction, manufacturing errors can also play a significant role on gear tooth wear patterns. The previous models did not take these imperfections into account as well. Also missing in these studies is validation of the models through gear wear experiments.

The main objective of this study is to develop a wear prediction methodology of parallel axis gear pairs (spur and helical) having intentional surface modifications and manufacturing/assembly related imperfections. This methodology will be validated through helical gear wear experiments. The impact of surface wear on gear contact stresses will also be investigated in detail to describe any influence wear might have on gear durability. For the prediction of contact pressures, a commercially available gear contact mechanics model will be employed. Quasi-static loading conditions will be assumed throughout this study. Gear tooth modifications and tooth manufacturing imperfections will be included in the model. A technique will be developed to import gear coordinate measurement data into the contact mechanics model for the inclusion of actual manufacturing imperfections.

While the methodology proposed here represents the current state of the art in terms of macro-level contact analysis of gears having intentional tooth geometry modifications and actual manufacturing errors, it is rather simplistic in terms of its treatment of wear. As mentioned earlier, the wear of contacting surfaces is dictated by a large number of geometric, operational and tribological parameters, all of which will be represented by an experimentally determined wear coefficient in this study. Similarly, having subject to dynamic conditions, gears experience larger and somewhat transient loads, causing contact pressures that are more complex than the ones predicted under static conditions. As a three-dimensional dynamic contact analysis of the required magnitude is not feasible with today's computers, enhancements to the wear in terms of dynamics and lubrication related effects will be left to future work [19,20].

2 Computational Wear Model

2.1 Wear Formulation. Gear contact involves combined rolling and sliding action of two mating surfaces that have varying geometry and loads. As in previous gear wear models [7,8,17], Archard's wear model will be employed here. With the assumption that the hardness values of the materials of contacting surfaces remain constant throughout the wear process, Archard's wear equation can be expressed for a local point on one of the contacting surfaces as

$$\frac{dh}{ds} = kP \qquad (2)$$

where k is a dimensional wear coefficient. Equation (2) can be integrated over s to find the wear depth h of any point on a gear contact surface. Although a number of mathematical relations to compute wear coefficient k for metallic sliding friction have been proposed in the past [21], k will be determined experimentally in this study, primarily due the complexity of the gear contact problem. It is clear from Eq. (2) that a prediction of the wear depth h requires the values of the contact pressure P and the sliding distance s of each point on gear tooth contact surfaces as a function of gear rotation.

The computational methodology employed here to predict the wear of contacting gear surfaces is shown in Fig. 1. The initial geometric description of the actual gear tooth surfaces serves as the initial state for the wear prediction. The use of actual profiles that contain manufacturing imperfections might be essential here as these variations are present especially in high-volume gear applications such as automotive systems. The tooth surface modifications must also be included in quantifying the initial contact of the gear surfaces. For this purpose, a gear coordinate measurement machine is used to obtain a large number of lead traces, each containing around 200 measurement points that are aligned using a single profile trace to obtain a three-dimensional measurement of the actual tooth surface. Accuracy and the repeatability of these measurements were found to be within $1-2$ μm that is sufficient for any wear evaluation. Measured geometries of each gear tooth contact surface are denoted by $(G_{ij}^{\kappa})^p$ and $(G_{ij}^{\kappa})^g$. Here, G_{ij} is the
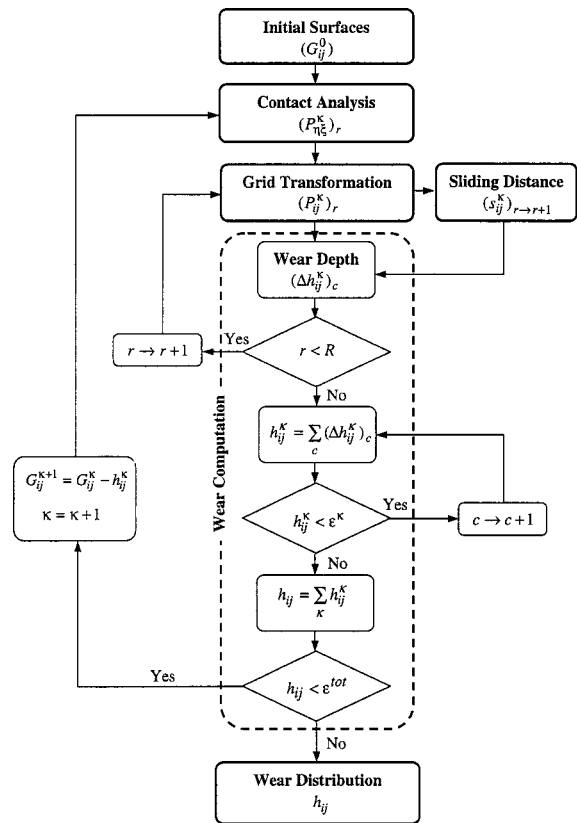

Fig. 1 Methodology used for the computation of wear

deviation of a surface point ij from the perfect involute surface, κ within the parenthesis indicates the number of geometry updates done so far in analysis. When $\kappa=0$, the tooth surface is brand new (no wear). The superscripts p and g outside the parenthesis denote the driving (pinion p) and driven (gear g) gears, respectively. By selecting points ij at the nodes of a predetermined surface grid, a discretized description of both contacting surfaces are obtained.

2.2 Computation of Contact Pressure Distribution. In Fig. 1, the second step in prediction of surface wear is a computation of the contact pressure at different rotational positions of the gears in mesh. The geometric data consisting of $(G_{ij}^{\kappa})^{p,g}$ are input to a deformable-body contact mechanics model to predict the instantaneous contact pressure distribution $(P_{\eta\xi}^{\kappa})^{p,g}$ at each rotational position $r=0,1,2,\ldots,R$. Here, R and the increment of the rotation are such that the amount of gear rotation achieved between positions $r=0$ to $r=R$ covers a complete wear cycle from the point where the tooth of interest enters the mesh zone for the first time to the point where it exists the mesh zone completely.

The prediction of $(P_{\eta\xi}^{\kappa})_r^{p,g}$ is itself a challenging task. A gear pair contact zone has several unique features, which make it difficult to use a conventional Finite Element (FE) model. The width of the contact zone is typically much smaller than the other geometric dimensions of the gear requiring a very fine mesh at the contact zone. As the contact moves, this fine mesh should follow the contact zone requiring a very refined grid throughout the active surface of the tooth. This increases the computational time required to predict the contact stresses at a given rotational position r significantly. Since a wear prediction would require the contact analysis to be performed at a large number of discrete positions (typically $R \geqslant 250$) as will be described later, such a refined conventional FE model becomes even less attractive. The contact mechanics model utilized in this study overcomes such difficulties by applying FE method in conjunction with a surface
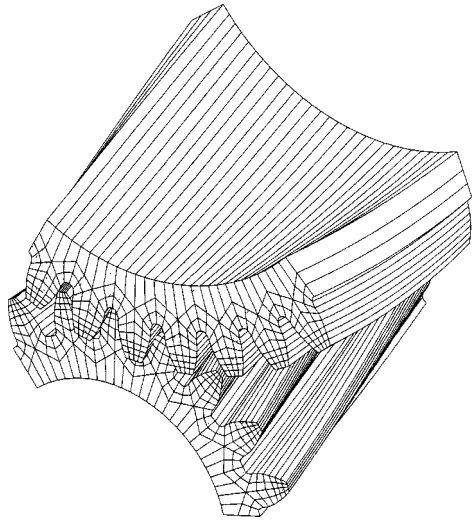
Fig. 2 A three-dimensional contact mechanics model of the example gear pair [22]

integral formulation. Here, only the features of the contact mechanics model relevant to the wear analysis will be outlined as readers will be referred to Vijayakar [22] for additional details.

To establish a fine grid only in the area of contact, the first task is to determine the areas that will be in contact at any given position when the gear pair is subjected to a torque. To determine that, a point at each contacting surface $\mathbf{X}^p$ and $\mathbf{X}^g$ must be identified such that the distance between the pinion and gear surfaces $\|\mathbf{X}^p - \mathbf{X}^g\|$ is minimum. The face width of the driving gear p is divided into $2N+1$ slices identified by the index $\xi = -N$ to N. For each slice ξ, a cross section of the driving gear p is taken in the middle of the slice, and a point is located on this slice that is closest to the surface of the driven gear g. This selection is carried out by using the undeformed geometry. A set of grid cells identified by the grid cell location indices $\eta\xi$, where $\eta = -M$ to M is set up centered on this closest point of slice ξ. The dimension of the grid cells in the profile direction is selected such that the actual contact zone is nearly 1/3 times smaller that the grid area defined. This way, at each rotational position $r = 0,1,2,\ldots,R$, a new moving surface grid $\eta\xi$ is established [22].

Figure 2 shows the contact mechanics model of the helical gear pair used in this study. Gears p and g have 34 and 22 teeth, respectively. The corresponding face width values are 30 and 26.7 mm. The gear pair has a normal module of 1.44 mm, pressure angle of 19 deg and helix angle of 20 deg. A seven-tooth segment of each gear was found to be sufficient to predict the stress state of the central tooth pair at different positions r [23]. For this particular gear pair, the total angle of rotation of the driving gear required for one tooth to go through a complete wear (contact) cycle is nearly 45 deg. Hence, analysis was carried out for a total of $R = 280$ positions with an angular increment of 0.16 degrees to obtain smooth wear distributions.

The pressure predictions of the contact mechanics model $(P_{\eta\xi}^\kappa)_r^{p,g}$ are given at nodal points $\eta\xi$ of a moving surface grid that follows the contact zone while gears rotate. The next task in Fig. 1, therefore, becomes a grid transformation that converts the pressures $(P_{\eta\xi}^\kappa)_r^{p,g}$ at the moving grid nodes $\eta\xi$ given by the position vector $(\mathbf{X}_{\eta\xi}^\kappa)_r^{p,g}$ to the pressures $(P_{ij}^\kappa)_r^{p,g}$ at nodes ij of a fixed surface grid that rotates with the gear tooth. This way, the contact pressure values $(P_{ij}^\kappa)_r^{p,g}$ are described at each fixed surface grid node ij located at $(\mathbf{X}_{ij}^\kappa)_r^{p,g}$ for any rotational position r and wear iteration κ.

The loaded flanks of the teeth forming the pair are discretized by $I+1$ equally spaced lead lines along the profile direction and
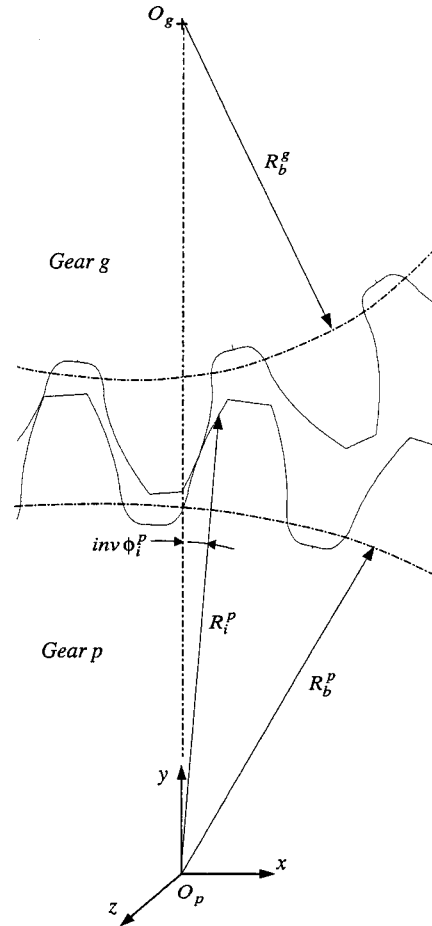

Fig. 3 Basic involute gear parameters and the coordinate frame

$J+1$ equally spaced profile lines along the lead direction. Hence, nodes of a fixed surface grid are defined at discrete locations ij where $i = 0,1,2,\ldots,I$ and $j = 0,1,2,\ldots,J$ resulting in $(I+1) \times (J+1)$ number of points representing the tooth contact surface of each gear. If the ith grid line of the tooth on the driving gear in profile direction has radius R_i^p, then angle $inv\,\phi_i^p$ defined in Fig. 3 can be described by using the relationships of involute gear geometry as

$$inv\,\phi_i^p = \tan\left[\cos^{-1}\left(\frac{R_b^p}{R_i^p}\right)\right] - \cos^{-1}\left(\frac{R_b^p}{R_i^p}\right) \tag{3}$$

where $inv\,\phi_i^p$ is the involute angle and R_b^p is the base circle radius. Position vector of a point R_i^p on the side edge of gear p ($j=0$) at the starting rotational position $r=0$ is given by

$$(\mathbf{X}_{i0})_{r=0}^p = \begin{bmatrix} R_i^p \sin(inv\,\phi_i^p) \\ R_i^p \cos(inv\,\phi_i^p) \\ 0 \end{bmatrix}. \tag{4}$$

As one moves away from this edge keeping the radius constant, the profile is rotated due to the helix angle only. The amount of this rotation at a distance $z^p = j\Delta z^p$ along the gear face from the edge is given by

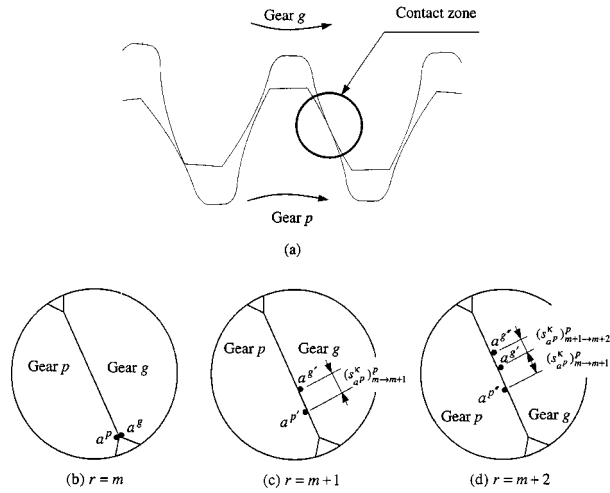$$\Delta\varphi_{ij}^p = \frac{j\Delta z^p \tan\psi_i^p}{R_i^p} \tag{5}$$

Fig. 4 Illustration of sliding distance of a point a^p on gear p at different positions r

where $\Delta z^p = F^p / J$, ψ_i^p is the helix angle at radius R_i^p, and F^p is face width of gear p. Hence, the position vector of any node ij on the fixed surface grid at $r = 0$ is given by

$$
(\mathbf{X}_{ij})_{r=0}^p = \begin{bmatrix} \cos \Delta \varphi_{ij}^p & \sin \Delta \varphi_{ij}^p & 0 \\ -\sin \Delta \varphi_{ij}^p & \cos \Delta \varphi_{ij}^p & 0 \\ 0 & 0 & 1 \end{bmatrix} (\mathbf{X}_{i0})_{r=0}^p + \begin{bmatrix} 0 \\ 0 \\ -j\Delta z^p \end{bmatrix}.
$$

$$(6)$$

Finally, if one incremental rotation of gear p from any position r to $r+1$ amounts to an angle $\Delta \theta^p$, then the position vector of node ij on gear p at the rth rotational position is given by

$$
(\mathbf{X}_{ij})_r^p = \begin{bmatrix} \cos(r\Delta \theta^p) & \sin(r\Delta \theta^p) & 0 \\ -\sin(r\Delta \theta^p) & \cos(r\Delta \theta^p) & 0 \\ 0 & 0 & 1 \end{bmatrix} (\mathbf{X}_{ij})_{r=0}^p .
$$

$$(7)$$

Equations (6) and (7) define the coordinates of every fixed grid node ij along the entire tooth surface at any given rotational position. The same procedure is applied to obtain the position vectors of the fixed grid points on the driven gear g as well.

As mentioned earlier, contact mechanics model provides the contact pressure $(P_{\eta\xi}^\kappa)_r^{p,g}$ at the center and corners of each cell $\eta\xi$ of its own moving grid for both gears p and g at every rotational position r of the gears in mesh. Any fixed grid node ij, which lies within any moving grid cell, is assigned a pressure value $(P_{ij}^\kappa)_r^{p,g}$ according to its distance weight from the four corners of that moving grid cell. All other fixed grid nodes that are not within the contact zone are assigned zero pressure values.

2.3 Computation of Sliding Distance. The sliding distance $(s_{ij}^\kappa)_{r \to r+1}^{p,g}$ is defined as the distance by which a point represented by node ij on one gear slides with respect to its corresponding point on the mating gear as gears rotate from position r to position $r+1$ after κ^{th} geometry update. Consider a fixed point a^p on the active tooth surface of gear p. Assume that the leading edge of contact reaches the point at a particular rotational position $r = m$ and contact zone passes through the point a^p in following incremental rotations. The sliding distance calculation becomes a matter of tracking the relative position of this point with respect to its mating point on the other gear. Focusing in the circled contact zone shown in Fig. 4(a) in the transverse plane of gears, Fig. 4(b) shows the start of wear cycle of a given point a^p at node ij on gear p as well as its mating point a^g on gear g. At this rotational position $r = m$, both a^p and a^g are at the leading edge of the

contact zone, experiencing a nonzero pressure for the first time since the beginning of loading cycle. Position vector of point a^p that lies on node ij of the fixed surface grid on gear p can be written as

$$
(\mathbf{X}_{a^p})_{r=m}^p = [x_{ij}, \quad y_{ij}, \quad z_{ij}]_{r=m}^p
$$

$$(8)$$

Since points a^p and a^g overlap in space at position $r = m$, the position vector of point a^g on the mating gear will be the same as that of point a^p

$$
(\mathbf{X}_{a^g})_{r=m}^g = (\mathbf{X}_{a^p})_{r=m}^p
$$

$$(9)$$

When the gears are rotated by one incremental rotation to position to $r = m + 1$, point a^p rotates about the center O^p of gear p. If one incremental rotation of gear p amounts to angle $\Delta \theta^p$, the position vector of a^p at $r = m + 1$ is given simply by a coordinate rotation transformation

$$
(\mathbf{X}_{a^p})_{r=m+1}^p = \begin{bmatrix} \cos \Delta \theta^p & \sin \Delta \theta^p & 0 \\ -\sin \Delta \theta^p & \cos \Delta \theta^p & 0 \\ 0 & 0 & 1 \end{bmatrix} (\mathbf{X}_{a^p})_{r=m}^p \quad (10)
$$

As illustrated in Fig. 4(c) at position $r = m + 1$, point a^g on gear g no longer overlaps with point a^p on gear p as gear g rotates about its center O^g. Position vector of point a^g can be obtained by first translating the coordinate frame from O^p to O^g (see Fig. 4), then rotating it by $\Delta \theta^g$, and finally translating it back to O^p where $\Delta \theta^g = -(Z^p / Z^g) \Delta \theta^p$. Here, Z^p and Z^g are the number of teeth of gears p and g, respectively. Accordingly, the position vector of point a^g on gear g at position $r = m + 1$ is given by

$$
(\mathbf{X}_{a^g})_{r=m+1}^g = \begin{bmatrix} \cos \Delta \theta^g & \sin \Delta \theta^g & 0 \\ -\sin \Delta \theta^g & \cos \Delta \theta^g & 0 \\ 0 & 0 & 1 \end{bmatrix} \left\{ (\mathbf{X}_{a^g})_{r=m}^g + \begin{bmatrix} 0 \\ -E \\ 0 \end{bmatrix} \right\}
$$
$$
+ \begin{bmatrix} 0 \\ E \\ 0 \end{bmatrix}
$$

$$(11)$$

where E is the center distance. Thus, relative sliding distance of point a^p defined on a fixed grid node ij on gear p while moving from position $r = m$ to $r = m + 1$ is given by

$$
(s_{a^p}^\kappa)_{m \to m+1}^p = \| (\mathbf{X}_{a^g})_{r=m+1}^g - (\mathbf{X}_{a^p})_{r=m+1}^p \|
$$

$$(12)$$

In order to generalize the above equation, consider the contact zone at the next position $r = m + 2$ as shown in Fig. 4(d). Here, as gears rotate more the points of interest a^p and a^g move further away from each other. Relative sliding distance increment as gears rotate from position $r = m + 1$ to $r = m + 2$ is equal to the distance between a^p and a^g minus $(s_{a^p}^\kappa)_{m \to m+1}^p$. If point a^p enters the contact zone at position $r = m$ and remains within contact zone until position $r = t$, the sliding distance that occurs when gears rotate from any position r to $r + 1$ can be given in general terms as

$$
(s_{a^p}^\kappa)_{r \to r+1}^p = \begin{cases} \left| \left\| (\mathbf{X}_{a^g})_{r+1}^g - (\mathbf{X}_{a^p})_{r+1}^p \right\| - \sum_{q=m}^r (s_{a^p}^\kappa)_{q-1 \to q}^p \right|, \\ \qquad m \leq r \leq t \\ 0, \quad 0 \leq r < m \ \ or \ \ t < r < R \end{cases}
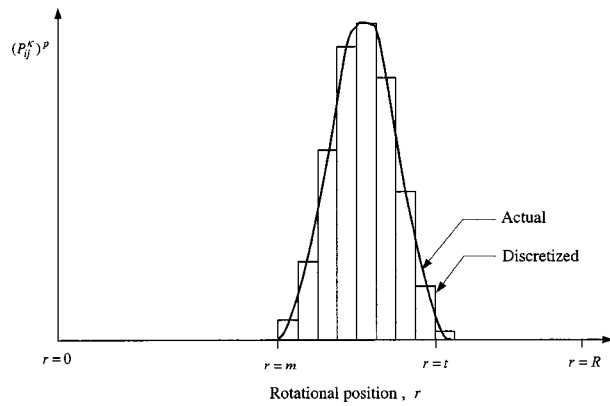$$

$$(13)$$

Fig. 5 Illustration of the change of contact pressure $(P_{ij}^{\kappa})^p$ of a point ij as a function or r

Noting that for the point a^p represented by a discretized node ij, $(P_{ij}^{\kappa})_r^p$ becomes nonzero for the first time at position $r=m$ and remains nonzero up to $r=t$ as illustrated schematically in Fig. 5. Here, the solid continuous line represents the actual contact pressure $(P_{ij}^{\kappa})^p$ that the point experiences. The angular span needed for the contact zone to pass through the point ij is very small since the width of the contact ellipse is very narrow. It is also clear that $(P_{ij}^{\kappa})^p$ varies significantly, starting from zero and reaching its maximum when the major axis of the contact (line of contact) is at point ij. Therefore, it is vital to have a large R (small $\Delta\theta^p$) such that $(P_{ij}^{\kappa})_r^p$, which is a discretized snapshot of $(P_{ij}^{\kappa})^p$ at position r in Fig. 5, is refined enough to capture the pressure history of the point. In Fig. 5, R is such that there are nine discrete positions available to approximate $(P_{ij}^{\kappa})^p$ when point ij is in the contact zone. It is also noted in Eq. (13) that the sliding distance is not a function of the size of the rotational increment. Reducing step size results in reduced sliding distance from one rotational position to the next, but the total sliding experienced by the point of interest as it goes through the contact remains the same since the point remains within the contact zone for more incremental positions. The same is true when the rotational increment is increased.

The sliding distance calculations must be carried out only for those nodes with nonzero $(P_{ij}^{\kappa})_r^{p,g}$ for at least two consecutive rotational positions. Sliding distance calculations for node ij of gear p are continued as r is increased until $(P_{ij}^{\kappa})_r^{p,g}$ becomes zero again. In calculating the sliding distance of point a^g on gear g with respect to point a^p on gear p, the same procedure is repeated by applying Eq. (11) to (13), now for gear g.

2.4 Computation of Wear Depth. With $(P_{ij}^{\kappa})_r^{p,g}$ and $(s_{ij}^{\kappa})_{r\to r+1}^{p,g}$ in hand, the wear depth occurring at each node ij of the fixed surface grid ($i=0,1,2,\ldots,I$ and $j=0,1,2,\ldots,J$) during one wear cycle can be computed by using Eq. (2). As shown in Fig. 1, if the maximum wear depth accumulated after the κth geometry update is less than a predetermined wear amount ε^{κ} that warrants a pressure distribution update, accumulated wear depth is obtained by summing up wear depth for many cycles until it reaches ε^{κ}. As soon as maximum wear depth for each κ reaches ε^{κ} at any point on the tooth surface, the worn geometry of tooth surfaces is established and sent to the contact mechanics model for an update of pressure distribution $(P_{ij}^{\kappa})_r^{p,g}$. This iterative procedure is repeated until the maximum total wear depth on either of the two gears reaches a certain maximum allowable wear threshold value of ε^{tot}.

There are fixed surface grid nodes on the tooth that lie below the start of active profile and hence they never enter into the contact zone. For such points, the tooth sliding distance need not be calculated but assigned a value equal to zero. Given the pro-

cedure for discretizing the pressures over total sliding of any point on the tooth surface as illustrated in Fig. 5, Eq. (2) can be written in the form

$$(\delta h_{ij}^{\kappa})_{r\to r+1}^{p,g}=\frac{1}{2}k^{p,g}(s_{ij}^{\kappa})_{r\to r+1}^{p,g}\{(P_{ij}^{\kappa})_r^{p,g}+(P_{ij}^{\kappa})_{r+1}^{p,g}\} \quad (14)$$

for a fixed surface grid node ij as gears rotate from position r to $r+1$. Thus, the total wear depth reached at any point on the surface in c^{th} individual wear cycle is

$$(\Delta h_{ij}^{\kappa})_c^{p,g}=\sum_{r=0}^{R-1}(\delta h_{ij}^{\kappa})_{r\to r+1}^{p,g} \quad (15)$$

Equations (14) and (15) are applied continuously C^{κ} times until the maximum wear depth accumulated at any node of either one of the contacting surfaces after the κth pressure update equals ε^{κ}. Then, the wear amount at nodes ij of gears p and g accumulated after the κth pressure update can be written as

$$(h_{ij}^{\kappa})^{p,g}=\sum_{c=1}^{C^{\kappa}}(\Delta h_{ij}^{\kappa})_c^{p,g} \quad (16)$$

After carrying out the iterations until K^{th} geometry update ($\kappa=0,1,2,\ldots,K$) when a point on either gear surface reaches the maximum allowable wear value of ε^{tot}, the cumulative wear depth distribution at node ij just before the Kth update is given by

$$h_{ij}^{p,g}=\sum_{\kappa=1}^{K}(h_{ij}^{\kappa})^{p,g} \quad (17)$$

Finally, the total number of wear cycles resulting in the accumulation of wear becomes

$$C^{\text{tot}}=\sum_{\kappa=1}^{K}C^{\kappa}. \quad (18)$$

3 Wear Model Predictions

A typical automotive transmission external helical gear pair will be used to demonstrate the features of the wear model and to characterize the wear process. The contact mechanics model of this pair was shown earlier in Fig. 2. This gear pair is used in a transverse, front-wheel-drive automatic transmission final drive planetary gear set. When operated in a counter-shaft configuration with the gear rotational centers fixed, the ratio of wear cycles of mating gear pair is inversely proportional to ratio of number of teeth. For this system, the ratio of wear cycles of gear p to those of gear g is equal to $Z^p/Z^g=34/22=1.545$. In other words, for every complete input (gear p) rotation, a tooth on gear p goes through one complete wear cycle while a tooth on gear g completes 1.545 wear cycles.

3.1 Wear of an Unmodified Helical Gear Pair. For the first example case, both gears p and g were assumed to have perfect involute profiles with no modifications and manufacturing imperfections. An input torque of 165 N-m was used. Wear threshold was kept at $\varepsilon^{\kappa}=2$ μm throughout the analysis. In other words, geometry and pressure updates are carried out in 2-micron increments and the simulation is terminated after eight geometry updates. A number of analyses were performed using different ε^{κ} values to determine that ε^{κ} values below 2 μm resulted in very slight improvements for the application considered [23]. Also considering that a 280-position contact analysis after each geometry update took several hours of computation on a high-end personal computer and it was not possible to measure surface profiles with accurately beyond 1 μm wear, a threshold value $\varepsilon^{\kappa}=2$ μm or larger became a practical value. Since the values of the wear coefficient k will be determined experimentally in the next section,
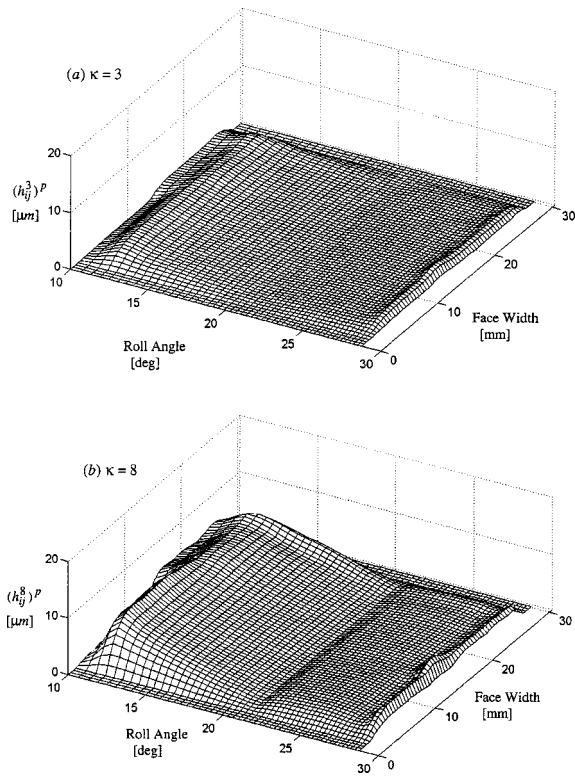
Fig. 6 Wear depth of gear p having no tooth surface modifications after geometry updates of (*a*) $\kappa=3$ and (*b*) $\kappa=8$; $\varepsilon^\kappa=2\,\mu$m
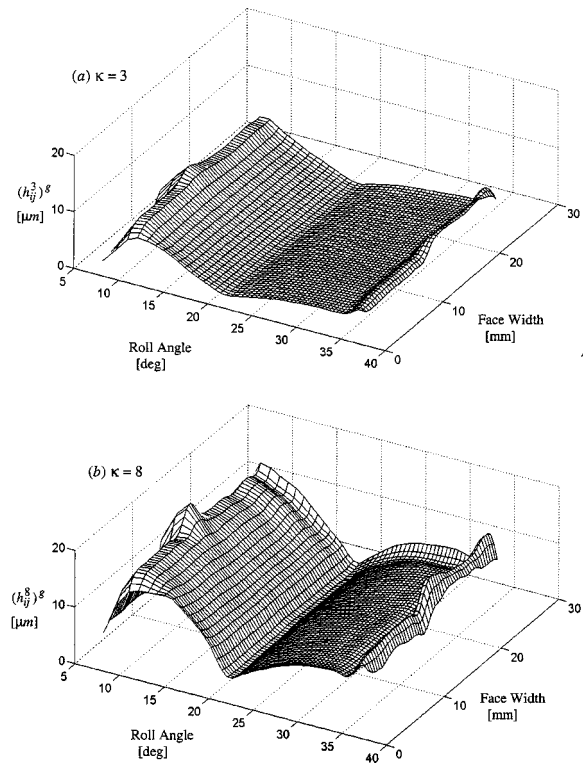

Fig. 7 Wear depth of gear g having no tooth surface modifications after geometry updates of (*a*) $\kappa=3$ and (*b*) $\kappa=8$; $\varepsilon^\kappa=2\,\mu$m

an arbitrary wear coefficient was employed in this analysis. In addition, the same value of k was used for both gears. Figures 6 and 7 show absolute wear distributions of gears p and g, respectively, after geometry updates of $\kappa=3$ and 8. The inverse of these images can be considered as the deviations of the tooth profiles from perfect involute since wear is material removal. It is noted here that wear amounts remain uniform in lead direction (face width) since there are no lead deviations (lead error or lead crown modification) present. This is especially true for gear g whose face width is 3.68 mm narrower than that of gear p. Therefore, the entire tooth surface along the face width of g comes to contact wearing off uniformly in lead direction. On the other hand, the wear at the edges of gear p in the lead direction taper off to zero since there exists an area at each side that does not experience any contact due to the excess face width that gear p has.

Also evident from Figs. 6 and 7 is that the wear amounts are negligible at roll angles of 21 deg of gear p and g along the involute direction. This is because the pitch line lies at these roll angles. At the pitch line, the gear contact experiences purely rolling (zero sliding distance) resulting in no wear. The most significant wear is observed in the dedendum region of driving gear, reaching the maximum wear amount quite near the start of active profile. For gear p, the ratio of the maximum dedendum wear to the maximum addendum wear is nearly 2. Meanwhile the addendum wear of gear g is quite significant. In addition, after the eighth pressure update, the maximum wear of gear g in Fig. 7(*b*) is about 16 μm while it is 8 μm in Fig. 6(*b*) for gear p, primarily due to the fact that the wear cycle rate of gear p is 1.545 times higher. In addition, the sudden increases in wear at the tip of each gear can be attributed to the rounding of the tip. Numerical difficulties can also contribute to such behavior since the prediction of contact stresses near the tip and the edges is the most challenging [22].
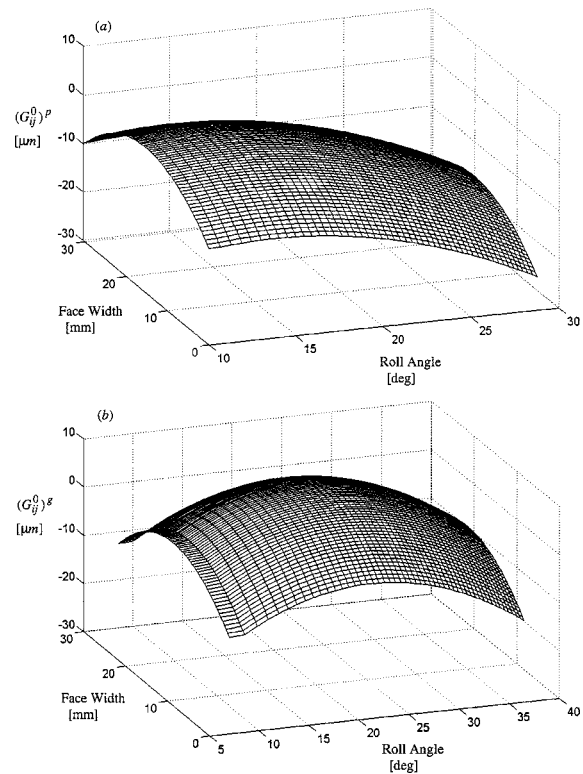

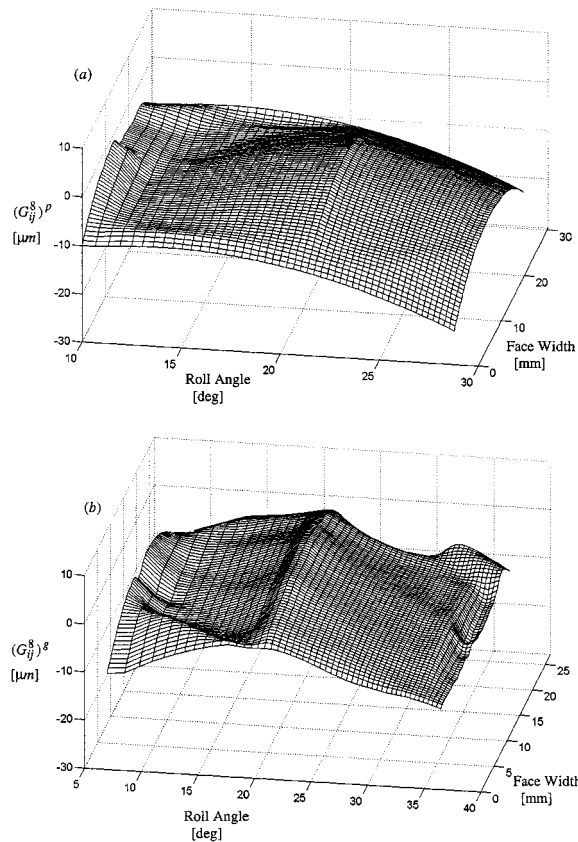**Fig. 8** Initial surfaces of (*a*) gear p and (*b*) gear g of a modified pair

Fig. 9 Worn surfaces of (*a*) gear *p* and (*b*) gear *g* having tooth surface modifications after geometry update of $\kappa=8$; $\varepsilon^{\kappa} =2$ μm

Fig. 10 Cumulative pressure contours of gear *p*, (*a*) $(P_{ij}^0)^p$ and (*b*) $(P_{ij}^8)^p$; $\varepsilon^{\kappa}=2$ μm

3.2 Wear of a Modified Helical Gear Pair. Next, the same gear pair was analyzed now with a number of lead and profile modification in the form of involute slope, involute crown and lead crown to reflect typical modification schemes of automotive helical gears. Figures 8(*a*) and 8(*b*) shows the initial profile geometries $(G_{ij}^0)^p$ and $(G_{ij}^0)^g$. All of the parameters were kept the same as the previous section including the torque and wear threshold values. Deviation of worn surfaces of gears *p* and *g* from a perfect involute profile $((G_{ij}^{\kappa})^p$ and $(G_{ij}^{\kappa})^g)$ are shown in Figs. 9(*a*) and 9(*b*), respectively, after the geometry update of $\kappa=8$. Maximum wear occurs in the middle of the tooth along the face width maximum pressure shifts towards center of the face width due to heavy lead crown applied to both tooth surfaces. In addition, a 13 μm involute slope applied to gear *p* causes larger wear amounts at the dedendum of gear *p* and addendum of gear *g*. The maximum wear depth values after the eighth geometric update in Fig. 9(*a*) and 9(*b*) are 8 μm for gear *p* at its dedendum and 14 μm for gear *g* at its addendum. A certain flattening of the crowned surfaces in lead direction is noted. Comparing Figs. 8 and 9 to Figs. 6 and 7 indicates conclusively that the wear characteristics of any modified gear pair is significantly different than its unmodified equivalent, suggesting that gear modifications must be included.

Another way to describe the influences of gear modifications on wear is to investigate its effect on the contact pressures $(P_{ij}^{\kappa})^p$ and $(P_{ij}^{\kappa})^g$ as the surfaces wear. In Fig. 10, the cumulative maximum contact pressure contours of contact surfaces of gears *p* corresponding to Figs. 8 and 9 are shown. Here, it is obvious from Fig. 10(*a*) for $\kappa=0$ (unworn surfaces) that the areas at the corners of both gears do not experience any contact initially. Pressures are distributed uniformly along the areas of contact at this early stage. Maximum pressure is around 1680 MPa at the pitch line and 1790
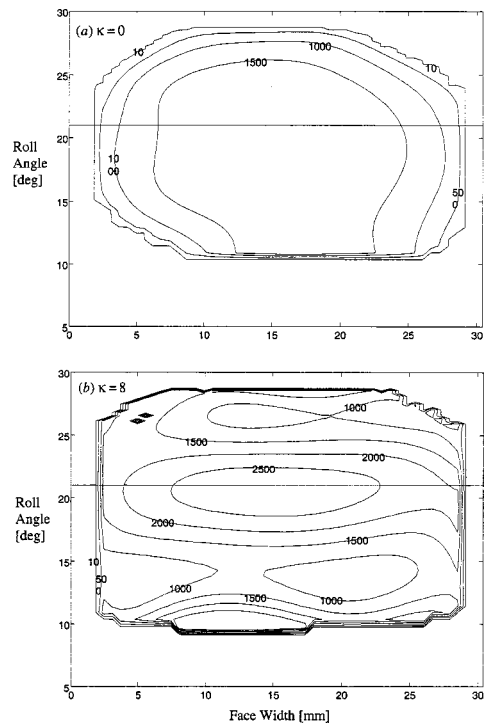
MPa at a roll angle of 15 deg below pitch line of gear *p*. As the surfaces wear, noncontacting areas at the corners get smaller. In addition, the areas along the pitch line experience significantly more pressures at the expense of the areas worn heavily as shown in Fig. 10(*b*). For $\kappa=8$, the maximum contact pressures are 2825 MPa at the pitch point and 1230 MPa at 15 deg roll angle.

3.3 Wear of a Modified Helical Gear Pair With Manufacturing Imperfections. Finally, the same modified gear pair was considered with tooth surface imperfections originating from the manufacturing processes (cutting and heat treatment) employed. An actual pair of helical gears (whose nominal geometry shown in Fig. 8) was inspected on a gear coordinate measurement machine to quantify the initial surface geometries as shown in Figs. 11(*a*) and 12(*a*) for gears *p* and *g*, respectively. A methodology was developed for this purpose that requires a number of lead and involute measurements to create a surface formed by 201 nodes in the lead direction and 51 nodes in involute direction. Figures 11(*b*) and 12(*b*) show the worn surfaces of gears *p* and *g* after $\kappa=8$. A comparison of these results in Figs. 11 and 12 indicates that such manufacturing imperfections can indeed significantly alter the wear characteristics.

4 Comparison to Experiments

As any theoretical model, predictions of the wear model proposed in this study must be validated through gear wear experiments. As actual gear experiments are very costly and take long periods of time, a limited amount of data is presented here. The external gear meshes (sun-planet) of a planetary gear set were utilized for validation. The main reason for selecting a planetary helical system for validation was not only to demonstrate that the model is capable of handling other, more complicated kinematic configurations, but also due to the availability of a planetary gear set durability test machine and gear specimens for this particular gear set.

The first test was used to determine the value of *k* and the measured wear values of the subsequent tests were compared to the model predictions obtained using the same *k* value. Consider-
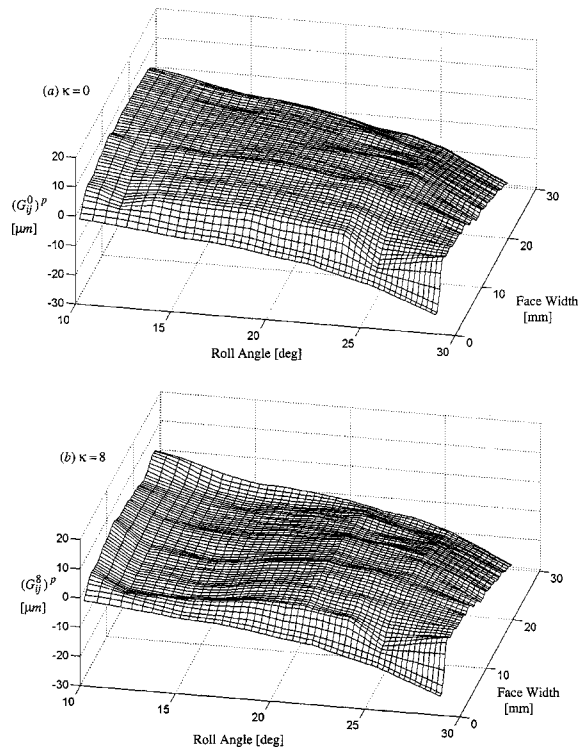
Fig. 11 Tooth surfaces of gear *p* (*a*) initial measured surface having both tooth surface modifications and manufacturing errors, and (*b*) worn surface after $\kappa=8$; $\varepsilon^\kappa=2$ μm
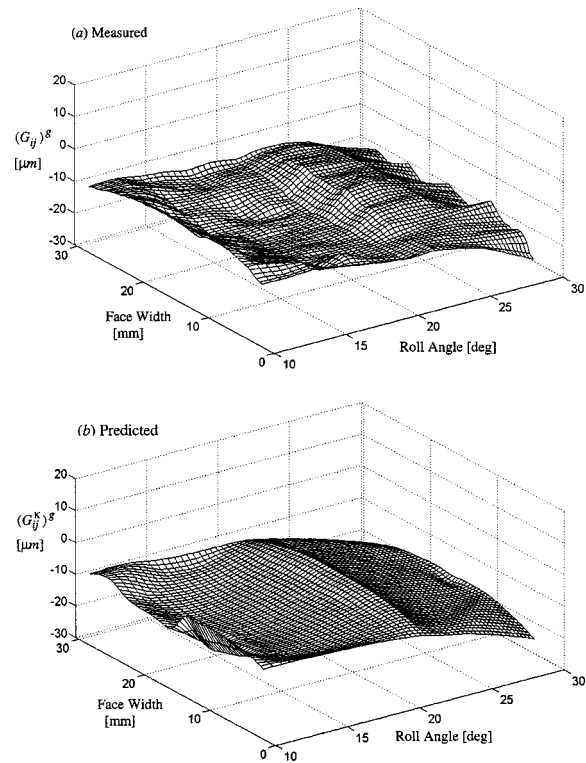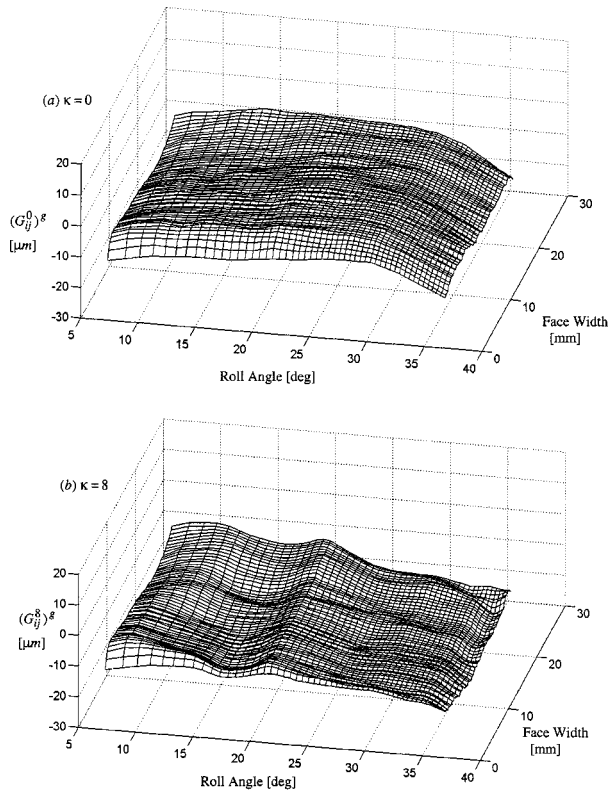

Fig. 12 Tooth surfaces of gear *g* (*a*) initial measured surface having both tooth surface modifications and manufacturing errors, and (*b*) worn surface after $\kappa=8$; $\varepsilon^\kappa=2$ μm

Fig. 13 Worn surfaces of gear *p* of test-1 after 27 million input cycles: (*a*) measurement, and (*b*) prediction

ing that all test specimens come from the same batch with the same material, heat treatment, and manufacturing processes, and also ensuring that each test was run at the same test conditions, the model predictions with the *k* value determined from the first test must be in agreement with the measured wear data.

The design parameters of sun and planet gears of the test gear set are identical to the previous example gear pair. Therefore, the contact mechanics model shown in Fig. 2 is valid for this pair as well. The sun gear serves as an input member while the planet carrier is the output. The internal gear is fixed to the case such that the gear set acts as a constant speed reduction device. In a parallel axis gear pair with fixed centers, the ratio of wear cycles of the mating gears is inversely proportional to ratio of number of teeth as in the previous section. In this planetary arrangement, however, the sun gear is in mesh with four identical planets and the planet carrier rotates by $Z^g/(Z^g+Z^i)=0.303$ per one input rotation where Z^i is the number of teeth of the internal gear. Accordingly, for every complete sun gear (input) rotation, teeth on the sun gear and a planet go through 2.785 and 1.077 wear cycles, respectively. In other words, the sun gear (driving gear *p*) experiences 2.585 times more wear cycles than a planet gear (driven gear *g*).

A "back-to-back" planetary gear test machine was used to perform the wear tests. Two identical planetary gear sets, one test gear set and a reaction gear set are connected to each other to form a power-circulation loop. Specifically, sun gears of both gear sets are connected to each other. Similarly both planet carriers are also connected. The internal gear of the test gear set is held stationary while a certain amount of constant torque is applied to the reaction internal gear, creating constant torque load. Both gear sets are then driven at a constant speed by a DC motor connected to the sun gears. A temperature-controlled supply of lubricant is maintained for lubrication as well as for heat dissipation.

The first test was run for 27 million input rotations. In Fig. 13(*b*), the predicted worn surface profile is shown here for $k=9.65\times10^{-19}$ m²/N, which was chosen so the predicted maximum wear depth was equal to the measured maximum wear depth
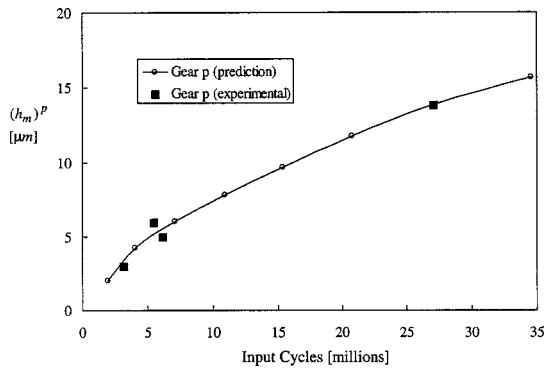
Fig. 14 Comparison of measured and predicted maximum wear depth values as a function of input cycles; $k = 9.65(10)^{-19}$ m²/N

of 14 μm. The wear in the dedendum region of the sun gear is more significant in both figures. The maximum wear amounth is observed in the midplane of the gears at nearly 15 deg roll angle. No wear is predicted at the pitch line (21 deg roll angle) while measured surface of Fig. 13(*a*) has a slight amount of wear in the vicinity of the pitch line. This might be due to the fact that the sun gear is allowed to float radially resulting in a variation of the operating center distance.

Next, three other wear tests were run to different total cycles and then simulated by the same k value (9.65×10^{-19} m²/N) obtained experimentally from the first test. The measured and predicted worn sun gear tooth surfaces for these three additional cases were found to be in good agreement both in terms of wear depth distributions and maximum wear depth. Comparison of predicted maximum wear depths with those measured on the sun gear is shown in Fig. 14, which indicates that wear rate starts decreasing as the gears wear. In agreement with the first test, the point of maximum wear for these three test were again located in the mid plane of the gears at nearly 15 deg roll angle. In summary, it can be stated from Figs. 13 and 14 that the model predictions are in good agreement with the experimental data.

5 Conclusion

In this study, a methodology that combines a contact analysis model and a wear prediction model to describe the evaluation of tooth surface wear of spur and helical gear pairs. The wear model used assumes that the change of wear rate is proportional to the product of contact pressure and the sliding distance. The methodology proposed here employs these two models iteratively to predict the progression of wear of contacting surfaces incrementally. Based on the analysis results and the experiments, the following conclusions can be made:

• The predictions of the proposed wear methodology and the experimental data agree well with each other, suggesting that, in spite of being a simple one, the wear model employed here is sufficient for most engineering applications provided that the contact pressures are predicted reasonably well.
• The initial geometry of the mating tooth surfaces impacts the wear behavior significantly. Therefore, designed tooth modifications must be included in the prediction of wear. Likewise, manufacturing imperfections must also be taken into account unless the gears are of high precision.

This methodology can be applied to other types of gear such as hypoid and spiral bevel gear sets that have significant sliding ac-

tion. It is also desirable to perform detailed parametric studies by using this methodology to quantify the influence of basic gear design parameters and tooth profile modifications to aid gear designer on how to minimize surface wear. The current work of these authors include enhancements to the wear model to eliminate the need for an empirical wear coefficient and addition of a dynamic gear contact analysis model to account for the coupling between the dynamic effects and wear.

References

[1] Choy, F. K., Polyshchuk, V., and Zakrajsek, J. J., Handschuh, R. F., and Townsend, D. P., 1996, "Analysis of the Effects of Surface Pitting and Wear on the Vibration of a Gear Transmission System," Tribol. Int., **29**, pp. 77–83.
[2] Mackaldener, M., Flodin, A., and Andersson, S., 2001, "Robust Noise Characteristics of Gears Due to their Applications, Manufacturing Errors and Wear," *JSME International Conference on Motion and Power Transmission*, MPT 2001, Fukuoka, Japan, 21–26.
[3] Kuang, J. H., and Lin, A. D., 2001, "The Effect of Tooth Wear on the Vibration Spectrum of a Spur Gear Pair," ASME J. Vibr. Acoust., **123**, pp. 311–317.
[4] Chen, Y., and Matubara, M., 2001, "Effect of Automatic Transmission Fluid on Pitting Fatigue Strength of Carborized Gears," *JSME International Conference on Motion and Power Transmission*, MPT 2001, Fukuoka, Japan, 151–156.
[5] Cioc, C., Cioc, S., Kahraman, A., and Keith, T. G., 2002, "A Deterministic Elastohydrodynamic Lubrication Model of High-Speed Transmission Components," Tribol. Trans., **45**, pp. 556–562.
[6] Wu, S., and Cheng, H. S., 1993, "Sliding Wear Calculation in Spur Gears," ASME J. Tribol., **115**, pp. 493–503.
[7] Flodin, A., and Andersson, S., 1997, "Simulation of Mild Wear in Spur Gears," Wear, **207**, pp. 123–128.
[8] Flodin, A., and Andersson, S., 2000, "Simulation of Mild Wear in Helical Gears," Wear, **241**, pp. 123–128.
[9] Rabinowicz, E., 1995, *Friction and Wear of Materials*, 2nd ed., John Wiley, New York.
[10] Archard, J. F., 1953, "Contact of Rubbing Flat Surfaces," J. Appl. Phys., **24**, pp. 981–988.
[11] Hsu, S. M., Shen, M. C., and Ruff, A. W., 1997, "Wear Prediction of Metals," Tribol. Int., **30**, pp. 377–383.
[12] Williams, J. A., 1999, "Wear Modeling: Analytical, Computational and Mapping: A Continuum Mechanics Approach," Wear, **225**, pp. 1–17.
[13] Zhao, Y. W., Liu, J. J., and Zheng, L. Q., 1992, "The Friction and Wear Model of Steels and their Probable Statistic Calculations," Tribol. Trans., **35**, pp. 673–678.
[14] Kato, K., 1997, "Abrasive Wear of Metals," Tribol. Int., **30**, pp. 333–338.
[15] Sawyer, W. G., 2001, "Life Prediction for a Simple Cam Including Couple Evolution of Wear and Load," Lubr. Eng., September, pp. 31–36.
[16] Priest, M., Dowson, D., and Taylor, C. M., 1999, "Predictive Wear Modeling of Lubricated Piston Rings in a Diesel Engine," Wear, **231**, pp. 89–101.
[17] Flodin, A., and Andersson, S., 2001, "A Simplified Model for Wear Prediction in Helical Gears," Wear, **249**, pp. 285–292.
[18] Wagaj, P., and Kahraman, A., 2002, "Effect of Tooth Profile Modifications on Helical Gear Durability," ASME J. Mech. Des., **124**, pp. 501–510.
[19] Krantz, T., and Kahraman, A., 2004, "An Experimental Investigation of the Influence of the Lubricant Viscosity and Additives on Gear Wear," Tribol. Trans., **47**, pp. 138–148.
[20] Yuksel, C., and Kahraman, A., 2003, "Dynamic Tooth Loads of Planetary Gear Sets Having Tooth Profile Wear," Mech. Mach. Theory, accepted for publication.
[21] Challen, J. M., and Oxley, P. L. B., 1986, "Prediction of Archard's Wear Coefficient for Sliding Metallic Sliding Friction Assuming Low Cycle Fatigue Wear Mechanism," Wear, **111**, pp. 275–288.
[22] Vijayakar, S., 1991, "A Combined Surface Integral and Finite Element Solution for a Three-dimensional Contact Problem," Int. J. Numer. Methods Eng., **31**, pp. 525–545.
[23] Bajpai, P., 2002, "A Wear Prediction Model for Parallel-Axis Gear Pairs," M.S. thesis, The University of Toledo, Toledo, OH.